

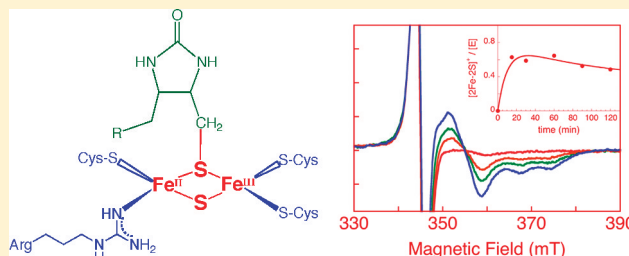
# Reduction of the [2Fe–2S] Cluster Accompanies Formation of the Intermediate 9-Mercaptodethiobiotin in *Escherichia coli* Biotin Synthase

Andrew M. Taylor,<sup>†</sup> Stefan Stoll,<sup>‡</sup> R. David Britt,<sup>‡</sup> and Joseph T. Jarrett<sup>\*,†</sup>

<sup>†</sup>Department of Chemistry, University of Hawaii at Manoa, Honolulu, Hawaii 96822, United States

<sup>‡</sup>Department of Chemistry, University of California, Davis, Davis, California 95616, United States

**ABSTRACT:** Biotin synthase catalyzes the conversion of dethiobiotin (DTB) to biotin through the oxidative addition of sulfur between two saturated carbon atoms, generating a thiophane ring fused to the existing ureido ring. Biotin synthase is a member of the radical SAM superfamily, composed of enzymes that reductively cleave *S*-adenosyl-L-methionine (SAM or AdoMet) to generate a *S'*-deoxyadenosyl radical that can abstract unactivated hydrogen atoms from a variety of organic substrates. In biotin synthase, abstraction of a hydrogen atom from the C9 methyl group of DTB would result in formation of a dethiobiotinyl methylene carbon radical, which is then quenched by a sulfur atom to form a new carbon–sulfur bond in the intermediate 9-mercaptodethiobiotin (MDTB). We have proposed that this sulfur atom is the  $\mu$ -sulfide of a [2Fe–2S]<sup>2+</sup> cluster found near DTB in the enzyme active site. In the present work, we show that formation of MDTB is accompanied by stoichiometric generation of a paramagnetic FeS cluster. The electron paramagnetic resonance (EPR) spectrum is modeled as a 2:1 mixture of components attributable to different forms of a [2Fe–2S]<sup>+</sup> cluster, possibly distinguished by slightly different coordination environments. Mutation of Arg260, one of the ligands to the [2Fe–2S] cluster, causes a distinctive change in the EPR spectrum. Furthermore, magnetic coupling of the unpaired electron with <sup>14</sup>N from Arg260, detectable by electron spin envelope modulation (ESEEM) spectroscopy, is observed in WT enzyme but not in the Arg260Met mutant enzyme. Both results indicate that the paramagnetic FeS cluster formed during catalytic turnover is a [2Fe–2S]<sup>+</sup> cluster, consistent with a mechanism in which the [2Fe–2S]<sup>2+</sup> cluster simultaneously provides and oxidizes sulfide during carbon–sulfur bond formation.



Biotin synthase (BS) is an *S*-adenosyl-L-methionine (AdoMet) radical enzyme that catalyzes the oxidative addition of a sulfur atom between the C6 methylene and C9 methyl groups of dethiobiotin (DTB), generating the thiophane ring of biotin.<sup>1–3</sup> In our working mechanism (Figure 1A), catalysis is initiated by one-electron reduction of AdoMet sulfonium, generating methionine and a *S'*-deoxyadenosyl radical (dA<sup>•</sup>). This reactive radical is a strong oxidant that abstracts a hydrogen atom from the C9 methyl of DTB,<sup>4</sup> generating a putative DTB-centered carbon radical that is then quenched by a sulfur atom derived from within the enzyme.<sup>5–7</sup> The product of this initial reaction sequence, 9-mercaptodethiobiotin (MDTB),<sup>8</sup> remains tightly bound to the enzyme while *S'*-deoxyadenosine (dAH) and methionine dissociate and a second equivalent of AdoMet binds (Figure 1A). A similar reaction sequence directed at the C6 methylene of MDTB closes the thiophane ring. While the overall chemical stoichiometry is now clearly established,<sup>9–11</sup> the electron stoichiometry depends on the chemical identity of the sulfur atom incorporated into biotin.

The structure of the BS homodimer shows that each monomer contains an ( $\alpha\beta$ )<sub>8</sub> barrel that encapsulates the presumed active site, containing AdoMet, DTB, and two FeS clusters.<sup>12</sup> In a structural motif shared with other AdoMet

radical enzymes, a [4Fe–4S]<sup>2+</sup> cluster is coordinated by Cys53, Cys57, and Cys60 within an extended loop between  $\beta$  strand 1 and  $\alpha$  helix 1. The fourth Fe atom of this cluster is coordinated by the amine and carboxylate of AdoMet,<sup>12,13</sup> positioning the sulfonium of AdoMet  $\sim 4$  Å from the cluster. The redox-active [4Fe–4S]<sup>2+/+</sup> cluster lies near the surface of the protein, and the presumed role for this cluster is to pass an electron from an external protein donor (flavodoxin in *E. coli*) into the AdoMet sulfonium, facilitating reductive cleavage of the C5'–S bond and generation of a *S'*-deoxyadenosyl radical. In addition to this cluster, a [2Fe–2S]<sup>2+</sup> cluster is bound deep within the ( $\alpha\beta$ )<sub>8</sub> barrel, with one Fe coordinated by Cys97 and Cys121 and the other Fe coordinated by Cys188 and Arg260.<sup>12</sup> The [2Fe–2S]<sup>2+</sup> cluster is bound  $\sim 4.6$  Å from DTB (Figure 1B), and we have proposed the  $\mu$ -sulfide from this cluster is the sulfur incorporated into DTB. Consistent with this proposal, elimination of this FeS cluster by site-directed mutagenesis of Cys97, Cys121, or Cys188 to Ala renders the enzyme inactive.<sup>14</sup> Further, BS in which the [2Fe–2S]<sup>2+</sup> cluster has been reconstituted with <sup>34</sup>S<sup>2–</sup> or Se<sup>2–</sup> incorporates ca. 60–70%

Received: July 7, 2011

Revised: August 18, 2011

Published: August 22, 2011

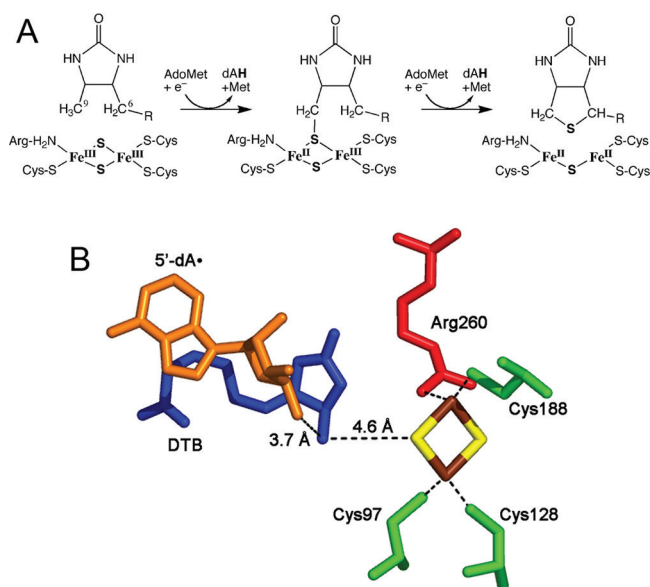


**Figure 1.** (A) The proposed biotin synthase reaction sequence. The reductive cleavage of AdoMet to dAH and methionine is coupled to abstraction of a hydrogen atom from C9 of DTB and formation of a new C–S bond in MDTB. We propose that the sulfur donor is the [2Fe–2S]<sup>2+</sup> cluster and that MDTB formation is coupled to transfer of an electron from the μ-sulfide into the cluster. Dissociation of dAH and methionine and binding of a second equiv of AdoMet is followed by a similar reaction sequence that closes the thiophane ring and results in complete reduction to an unstable diferric cluster. (B) The active site environment of the [2Fe–2S]<sup>2+</sup> cluster based on the 3.4 Å resolution crystal structure of *E. coli* BS in complex with AdoMet and DTB.<sup>12</sup> Cys97, Cys128, Cys188 (green), and Arg260 (red) coordinate the tetragonal [2Fe–2S]<sup>2+</sup> cluster (Fe<sup>3+</sup>, brown; S<sup>2-</sup>, yellow). C9 of DTB (blue) is ~4.6 Å (center-to-center) from the nearest μ-sulfide of this cluster. The C5' position of the transient dA• radical (orange) is generated ~3.7 Å away from C9 of DTB. Image generated with PyMol<sup>52</sup> using pdb file 1R30.

of the heavy-atom isotope into biotin, with the remainder of biotin incorporating <sup>32</sup>S presumably derived from buffer components.<sup>6,7</sup> In addition, formation of biotin is either accompanied by,<sup>15</sup> or possibly preceded by,<sup>16</sup> destruction of the [2Fe–2S]<sup>2+</sup> cluster, which might be expected if sulfide is extracted from the cluster during catalysis.

If sulfide derived from the [2Fe–2S]<sup>2+</sup> cluster quenches a dethiobiotinyl C9 methylene radical to generate the new C–S bond in MDTB, then the resulting molecule would contain an extra electron derived from sulfide that must be shed prior to or concurrent with bond formation. This electron could be transferred to either FeS cluster, resulting in the formation of a reduced paramagnetic FeS cluster that could be detected by electron paramagnetic resonance (EPR) spectroscopy. The [4Fe–4S]<sup>2+</sup> cluster readily undergoes chemical reduction by dithionite at  $E_m \approx -500$  mV (vs SHE),<sup>17,18</sup> generating a [4Fe–4S]<sup>+</sup> cluster that exhibits two signals detectable by EPR spectroscopy: a strong high-field  $S = 1/2$  signal with  $g = [2.04, 1.95, 1.91]$ <sup>19–21</sup> and a weak low-field  $S = 3/2$  signal at  $g = 5.6$ .<sup>20</sup> In the WT enzyme, the [2Fe–2S]<sup>2+</sup> cluster is not stable to chemical reduction. Treatment of WT BS containing one [2Fe–2S]<sup>2+</sup> cluster per monomer with dithionite leads to irreversible reduction and loss of this cluster with an apparent  $E_{red} = -430$  mV.<sup>18</sup> The product of this reduction process is a substoichiometric amount of the [4Fe–4S]<sup>+</sup> cluster<sup>18,20,22</sup> formed by dissociation and reassociation of the iron and

sulfide ions.<sup>21</sup> However, mutation of the nearby residues Asn153 or Asp155 to Ala appears to stabilize the reduced cluster. Chemical reduction of the [2Fe–2S]<sup>2+</sup> cluster with dithionite in these mutant enzymes results in formation of a semistable [2Fe–2S]<sup>+</sup> cluster exhibiting a high-field axial  $S = 1/2$  signal with  $g = [2.00, 1.91]$ .<sup>23</sup> This EPR signal has not been observed at any point during reduction of the WT enzyme.

A significantly different EPR signal has been observed during catalysis when BS is incubated with DTB, AdoMet, and a flavodoxin/FNR/NADPH reducing system. Ugulava et al. initially reported that room temperature incubation of BS with substrates and reducing system in the presence of excess iron and sulfide in the buffer resulted in slow development of a broad rhombic signal centered at  $g_{av} = 1.94$ .<sup>15</sup> Jameson et al. more thoroughly examined changes in the [2Fe–2S] cluster during turnover using EPR and Mössbauer spectroscopy<sup>16</sup> and reported formation and decay of a reduced paramagnetic FeS cluster exhibiting two broad overlapping rhombic signals ( $g = [2.010, 1.955, 1.880]$  and  $g = [2.000, 1.940, 1.845]$ ). Mössbauer spectra obtained in parallel contained a minor component ( $\delta \approx 0.25$  mm/s,  $\Delta E_Q \approx 5.5$  mm/s, ~10–20% of total <sup>57</sup>Fe species, estimated from Figure 1 in Jameson et al.<sup>16</sup>) attributed to a [2Fe–2S]<sup>+</sup> cluster. However, formation and decay of this [2Fe–2S]<sup>+</sup> cluster occurred on a time scale that was significantly faster than biotin formation, and the authors concluded that reduction and degradation of the [2Fe–2S]<sup>2+</sup> cluster likely occur before the catalytic reactions that generate biotin.<sup>16</sup>

We have since demonstrated that biotin formation proceeds in a stepwise manner, with conversion of DTB to MDTB within the first 5–10 min of turnover at 37 °C ( $k_1 = 0.07$  min<sup>-1</sup>), while conversion of MDTB to biotin lags initially and then proceeds at an apparent rate of  $k_{obs} = 0.05$  min<sup>-1</sup>.<sup>8,24</sup> However, a careful stoichiometric analysis suggests that only one monomer within the dimeric enzyme is undergoing turnover to form biotin, while the other monomer binds substrates but does not undergo a reaction, i.e., that the enzyme is half-site active.<sup>24</sup> Half-site activity leads to a lower-than-expected initial yield of products as well as a heterogeneous mixture of unreacted, partially reacted, and fully reacted FeS cluster-depleted enzyme monomers. In addition, the apparent rate of biotin formation is also subject to an unusual form of product inhibition,<sup>25</sup> in which dAH and methionine generated during the first half-reaction, conversion of DTB to MDTB, can cooperatively compete with AdoMet during the second half-reaction, preventing conversion of MDTB to biotin. This product inhibition would be most severe at high enzyme concentration ( $[E] \geq K_i \approx 20$  μM<sup>25</sup>) and would cause a significant disparity between the rate of formation of MDTB vs biotin. A stepwise mechanism for conversion of DTB to biotin, together with half-site activity and significant product inhibition of the second step, could explain the kinetic discrepancy between biotin formation and transformation of the [2Fe–2S]<sup>2+</sup> cluster reported by Huynh and co-workers.<sup>16</sup>

If the [2Fe–2S]<sup>2+</sup> cluster provides sulfide for conversion of DTB to MDTB, then we propose a mechanism in which the sulfide is simultaneously oxidized by inner-sphere electron transfer into the cluster, generating a transient paramagnetic FeS cluster in which MDTB may remain as a thiolate ligand (Figure 1A).<sup>1,8,11</sup> In this scenario, generation of a reduced FeS cluster should kinetically correlate with MDTB formation, not biotin formation. In the present work, we conduct assays with limiting AdoMet to enhance the production of MDTB over

biotin. By comparing spin concentrations determined from EPR to MDTB concentrations determined by HPLC analysis, we demonstrate a 1:1 stoichiometric correlation between production of MDTB and generation of a paramagnetic FeS cluster. We also confirm that the observed EPR signal is due to the  $[2\text{Fe}-2\text{S}]^+$  cluster, taking advantage of the unique Arg260 ligand to this cluster. EPR spectra of the active Arg260Met mutant enzyme show significant changes in  $g$  tensors consistent with a change in the coordination environment of the  $[2\text{Fe}-2\text{S}]^+$  cluster. ESEEM spectra of the WT enzyme show hyperfine coupling of  $^{14}\text{N}$  from the Arg260 ligand, and this coupling is lost in the Arg260Met mutant enzyme. The dual role of the  $[2\text{Fe}-2\text{S}]^{2+}$  cluster as both a substrate and redox cofactor is discussed within the broader context of the emerging subfamily of AdoMet radical C-S bond forming enzymes.

## MATERIALS AND METHODS

All reagents were obtained from commercial sources and used without further purification. AdoMet was purchased as the *p*-toluenesulfonate salt and contains ~15% 5'-methylthioadenosine and ~2% *S*-adenosyl-L-homocysteine. Expression and purification of wild-type<sup>18</sup> and Arg260Met<sup>17</sup> BS, as well as flavodoxin and His<sub>6</sub>-FNR,<sup>26</sup> were performed as previously described. The concentration of aerobically purified BS was estimated based on the absorbance spectrum of the  $[2\text{Fe}-2\text{S}]^{2+}$  cluster using  $\epsilon_{452} = 8400 \text{ M}^{-1} \text{ cm}^{-1}$  and confirmed by Bradford assay using BSA as a standard.<sup>18</sup>

**Preparation of EPR Samples Collected during BS Turnover.** Samples were prepared in a nitrogen-filled anaerobic glovebox operated at <1 ppm of O<sub>2</sub>. BS (25–125  $\mu\text{M}$  final dimer concentration) was added to vials containing 50 mM Tris HCl, 10 mM KCl, and 5 mM DTT, pH 8.0. The  $[4\text{Fe}-4\text{S}]^{2+}$  cluster was reconstituted by addition of 4 equiv of Na<sub>2</sub>S and FeCl<sub>3</sub>. Flavodoxin (20  $\mu\text{M}$ ), FNR (2  $\mu\text{M}$ ), NADPH (1 mM), and AdoMet (0–5 equiv) were added, and the sample was incubated for 10 min at room temperature. DTB (1–5 equiv) was added to initiate the reaction. Vials were incubated in the anaerobic chamber for 5–120 min, either at ambient temperature or in a 37 °C sand bath. At various intervals, samples were collected for HPLC analysis by removing 90  $\mu\text{L}$  of sample and quenching with 10  $\mu\text{L}$  of 4.5 M acetic acid/sodium acetate buffer, pH 4.5. At the same time, 300  $\mu\text{L}$  of sample was transferred to an EPR tube, and the tube was sealed, removed from the anaerobic chamber, and frozen in liquid nitrogen. EPR samples were shipped overnight on dry ice and then stored under liquid N<sub>2</sub> until spectra could be collected.

**Analysis of Biotin and MDTB by HPLC.** Acid-quenched samples were removed from the glovebox and chilled on ice for 10 min, and precipitated protein was removed by centrifugation for 10 min at 18000g. The supernatant was transferred to an HPLC autosampler vial and injected on a Waters Atlantis dC<sub>18</sub> reverse-phase column (3.0  $\times$  150 mm, 5  $\mu\text{m}$ ) equilibrated with 2% acetonitrile/H<sub>2</sub>O (0.1% H<sub>3</sub>PO<sub>4</sub>) at a flow rate of 0.7 mL/min. Sample components were eluted with a linear gradient from 2–25% acetonitrile over 25 min in the same buffer and detected by UV absorbance at 210 nm: biotin,  $t_{\text{R}} = 18$  min; DTB,  $t_{\text{R}} = 21$  min; MDTB,  $t_{\text{R}} = 23.6$  min.

The concentration of biotin and DTB in unknown samples was determined by comparison to commercial samples ( $\geq 98\%$  pure, Sigma), which were lyophilized to remove bound water and accurately weighed prior to preparation of stock solutions in stoichiometric NaOH solution. Extinction coefficients were

experimentally determined from UV spectra of multiple sample preparations: DTB,  $\epsilon_{210} = 870 \text{ M}^{-1} \text{ cm}^{-1}$ ; biotin,  $\epsilon_{210} = 1860 \text{ M}^{-1} \text{ cm}^{-1}$ . Since MDTB was not commercially available, the extinction coefficient of MDTB at 210 nm was estimated using the experimentally determined extinction coefficients for the amino acids alanine and cysteine to estimate the molar absorptivity of the thiol functional group. Solutions of each amino acid were gravimetrically prepared in deionized water, UV spectra were recorded, and  $\epsilon_{210}$  was calculated for each amino acid (note that this is a shoulder region, not a peak, in the UV spectrum). The increased absorbance of cysteine was used to determine  $\Delta\epsilon_{210}$  due to the thiol functional group. The extinction coefficient for MDTB was then calculated as  $\epsilon^{\text{MDTB}} = \epsilon^{\text{DTB}} + (\epsilon^{\text{Cys}} - \epsilon^{\text{Ala}})$ , yielding  $\epsilon_{210} = 1100 \text{ M}^{-1} \text{ cm}^{-1}$ . This method of estimation is likely to be reasonably accurate, as a similar estimation for biotin, using methionine instead of cysteine, yields  $\epsilon^{\text{biotin}} = \epsilon^{\text{DTB}} + (\epsilon^{\text{Met}} - \epsilon^{\text{Ala}}) = 2100 \text{ M}^{-1} \text{ cm}^{-1}$ , which compares well with the experimental  $\epsilon_{210} = 1860 \text{ M}^{-1} \text{ cm}^{-1}$ . Further, an examination of reference spectra of alkyl thiols and dialkyl thioethers in the NIST chemical database suggests that alkyl thiols have  $\epsilon_{210} = 250\text{--}300 \text{ M}^{-1} \text{ cm}^{-1}$ , while dialkyl thioethers have  $\epsilon_{210} = 800\text{--}1000 \text{ M}^{-1} \text{ cm}^{-1}$ . A sum of the extinction coefficients for DTB and alkyl thiols gives a similar estimate for the extinction coefficient MDTB of  $\epsilon_{210} = 1120\text{--}1170 \text{ M}^{-1} \text{ cm}^{-1}$ . Using these measured and estimated reference values, the concentration of MDTB in enzyme assays was then determined by HPLC analysis, using biotin as a standard, but then dividing the peak area of the biotin standard by the ratio of extinction coefficients:  $\epsilon_{\text{biotin}}/\epsilon_{\text{MDTB}}$  (210 nm) =  $1860/1100 = 1.69$ .

### Electron Paramagnetic Resonance Spectroscopy.

EPR spectra were measured at the CalEPR Center in the Department of Chemistry at the University of California, Davis. Continuous-wave (CW) spectra were collected using a Bruker ECS106 EPR spectrometer operating at X-band frequency (around 9.5 GHz). Typical sweep widths were 320–400 mT, although wider sweeps were also performed to rule out high-spin signals. Using a sample with a strong  $g \approx 2.04$  signal, spectra were collected with sample temperatures from 5 to 80 K and microwave power from 200 nW to 200 mW to examine the relaxation properties of signal components, yielding optimized conditions for observation of the FeS cluster signals at 20 K and 10 mW. Spectral simulations were performed using EasySpin.<sup>11</sup> Pulsed spectra were measured using a Bruker EleXsys E580 spectrometer. Three-pulse ESEEM ( $\pi/2\text{--}\tau\text{--}\pi/2\text{--}T\text{--}\pi/2\text{--}\tau\text{--}$ echo) spectra were acquired with 8 ns  $\pi/2$  pulses for several  $\tau$  values. The spin concentration of FeS clusters in BS samples was determined by comparison to samples of 50–200  $\mu\text{M}$  Cu<sup>2+</sup>–EDTA. For determination of the BS spin concentration, the flavodoxin FMN semiquinone signal ( $g = 2.005$ ) was saturated at high microwave power, and the residual signal was manually subtracted prior to spin integration.

## RESULTS

**MDTB Is Optimally Produced at Substoichiometric AdoMet Concentrations.** We have previously demonstrated that BS catalyzes a sequential reaction in which DTB is first converted to the intermediate MDTB, which remains tightly bound to the enzyme and is subsequently converted to biotin.<sup>8</sup> The reaction cycle requires two sequential hydrogen atom abstractions, first from C9 of DTB and then from C6 of MDTB, by 5'-dA<sup>•</sup> generated via reductive cleavage of AdoMet. Since we wished to measure changes in the EPR spectrum that

might correlate with formation of intermediates, we attempted to develop conditions that would generate a high concentration of the MDTB intermediate and we suspected would also yield a more intense EPR signal. Under typical assay conditions, a large excess of AdoMet (16 equiv per BS dimer) results in low yield of MDTB, with  $\sim 0.2$ – $0.3$  equiv per dimer formed in the first 5 min (Figure 2A, squares), falling off to  $\sim 0.1$ – $0.2$  equiv after 20

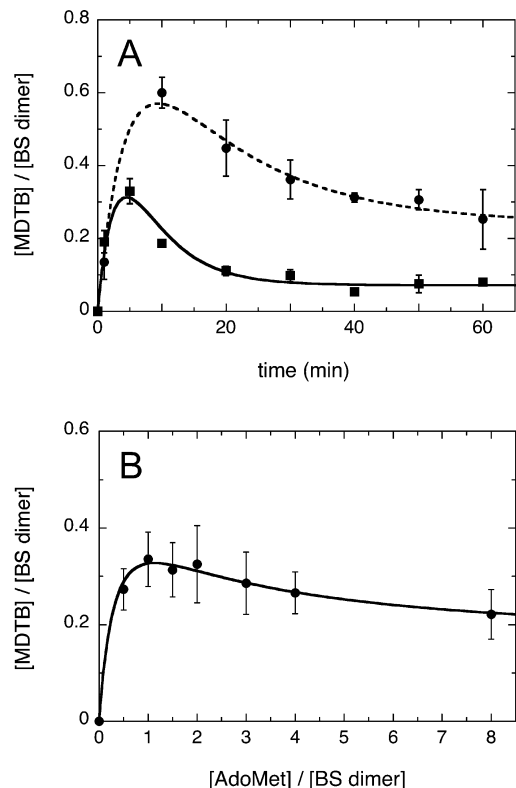


**Figure 2.** Catalytic intermediate MDTB is optimally formed at short reaction times and at limiting AdoMet concentrations. (A) Time dependence of MDTB formation. BS (12.5  $\mu\text{M}$  dimer) was assayed with DTB (200  $\mu\text{M}$ ) and AdoMet (circles, 100  $\mu\text{M}$ ; squares, 200  $\mu\text{M}$ ) at 37  $^{\circ}\text{C}$ . (B) AdoMet concentration dependence of MDTB formation. BS (25  $\mu\text{M}$  dimer) was assayed with DTB (200  $\mu\text{M}$ ) and AdoMet (25–400  $\mu\text{M}$ ) for 60 min at 37  $^{\circ}\text{C}$ . MDTB was determined by HPLC with UV detection at 210 nm, and the concentration was determined using a biotin standard and the conversion ratio  $\epsilon_{\text{biotin}}/\epsilon_{\text{MDTB}}$  (210 nm) = 1.69. Error bars represent the standard deviation of four samples.

min as this intermediate is converted to biotin. A decrease in the excess of AdoMet (8 equiv per dimer) results in an increased yield and prolonged lifetime of the MDTB intermediate (Figure 2A, circles). Initially, we had reasoned that limiting AdoMet to  $\sim 1$  equiv would result in conversion of DTB to MDTB, but there would be insufficient AdoMet to convert MDTB to biotin. However, when we varied the concentration of AdoMet over the range 0.5–8 equiv per dimer in a 60 min assay, we observed that maximally  $\sim 0.35$  equiv MDTB per dimer is formed when BS is incubated with 1 equiv of AdoMet (Figure 2B), but higher concentrations of AdoMet resulted in only a modest suppression of MDTB formation.

The inability to generate a stoichiometric amount of MDTB, even in the presence of limiting AdoMet, can be explained if AdoMet from unreacted active sites can rapidly dissociate and preferentially bind to active sites that contain MDTB; in other

words, if the  $K_m$  for AdoMet is lower for the second half-reaction with MDTB than for the first half-reaction with DTB (Figure 1A). Consistent with this interpretation, we have also found that MDTB formation in the first half-reaction is significantly slower in the presence of limiting AdoMet (data not shown), possibly due to incomplete saturation of AdoMet binding during the first half-reaction. Thus, we faced a trade-off in which the concentration of the intermediate could be increased somewhat by limiting the concentration of AdoMet, but the turnover rate is slowed under these conditions, possibly resulting in a decrease in the yield of intermediates and products.

**BS Turnover Is Accompanied by the Growth and Decay of a Multicomponent EPR Signal.** Having established that the BS reaction intermediate MDTB is maximally formed at  $\sim 0.3$ – $0.6$  equiv per BS dimer after incubation with 1–2 equiv AdoMet, we examined whether changes in the redox state of the BS FeS clusters might accompany MDTB formation, as predicted by our proposed mechanism. BS (100  $\mu\text{M}$  dimer) was preincubated for 5 min with DTT,  $\text{FeCl}_3$ , and  $\text{Na}_2\text{S}$  to reconstitute the  $[\text{4Fe-4S}]^{2+}$  cluster and for 10 min with flavodoxin, FNR, and NADPH to establish reducing conditions conducive to enzyme activity. DTB (400  $\mu\text{M}$ ) and AdoMet (100 or 400  $\mu\text{M}$ ) were then added to initiate BS turnover as in prior studies.<sup>8</sup> To ease handling of the large sample volumes required, the reaction was carried out in an open vial inside an anaerobic glovebox at ambient temperature ( $\sim 25$   $^{\circ}\text{C}$ ). At various time intervals (5–120 min), samples were collected in parallel for EPR and HPLC analysis: a 300  $\mu\text{L}$  sample was transferred to a quartz EPR tube, tightly capped, and frozen in liquid  $\text{N}_2$  until spectra could be collected several days later, while a 90  $\mu\text{L}$  sample was quenched with acid, the protein precipitate removed by centrifugation, and the supernatant analyzed for MDTB and biotin content by HPLC as described in the Materials and Methods. Within 5–10 min, the assay mixture developed a complex EPR spectrum in the range  $g = 1.84$ – $2.02$  ( $g_{\text{av}} \approx 1.94$ ), most likely due to overlapping signals from several spin systems (Figure 3A), including a narrow isotropic signal at  $g = 2.005$  from the flavin semiquinone radical in flavodoxin. A control sample with all reaction components except BS shows only this flavin semiquinone radical. While the flavin component gradually decays in intensity throughout the assay, the other components of the spectrum grow and decay in parallel, with strong intensity early in the time course and gradually weakening intensity at later times. The broad EPR spectrum with an approximately rhombic line shape, together with a relatively low  $g_{\text{av}}$  value of  $\sim 1.94$ , suggests that the spectrum is predominantly due to one or more  $[\text{2Fe-2S}]^+$  or  $[\text{4Fe-4S}]^+$  clusters.

To quantify the spin concentration in each sample, we compared double integrals of the spectra to those obtained from standards of  $\text{Cu}^{2+}$ -EDTA, with all spectra acquired under identical nonsaturating conditions. Prior to integration, the flavodoxin semiquinone contribution to each spectrum ( $\sim 2$ – $5$   $\mu\text{M}$  spin, mostly saturated at 10 mW microwave power) was manually subtracted using the control spectrum. The resulting spin concentrations (Figure 3B) correspond to the slow formation and partial decay of overlapping signals attributable to one or more reduced FeS clusters. At higher concentrations of AdoMet (4 equiv per BS dimer), the rate of formation of the EPR signal ( $k_{\text{obs}} \approx 0.1$   $\text{min}^{-1}$  at 25  $^{\circ}\text{C}$ ) appears to roughly correlate with the previously reported rate of MDTB formation ( $k_{\text{obs}} \approx 0.07$   $\text{min}^{-1}$  at 37  $^{\circ}\text{C}$ ).<sup>8</sup> However, at lower AdoMet

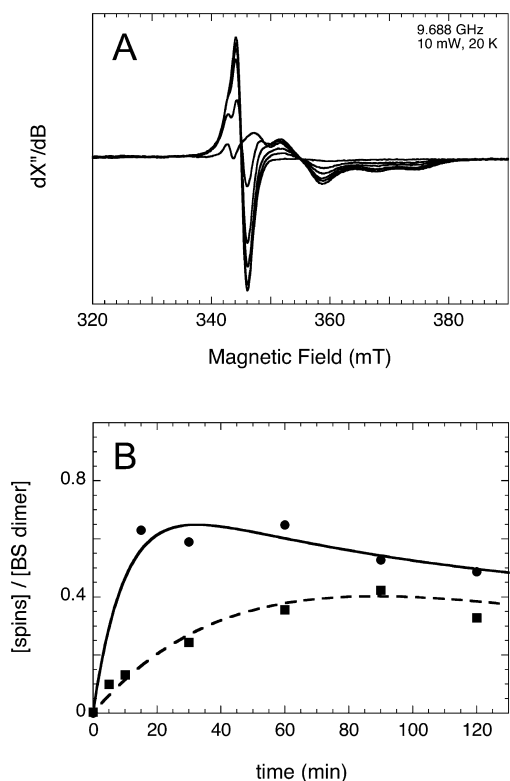


**Figure 3.** Formation of a reduced FeS cluster during the BS assay. (A) BS (100  $\mu\text{M}$  dimer) was incubated with DTB (400  $\mu\text{M}$ ) and AdoMet (100  $\mu\text{M}$ ) at ambient temperature ( $\sim 25^\circ\text{C}$ ) in an anaerobic glovebox, with other components of the assay as described in the Materials and Methods. At varying intervals (5–120 min), samples were transferred to an EPR tube and frozen in liquid  $\text{N}_2$ . Spectra were recorded at a 9.688 GHz, 10 mW, and 20 K. (B) EPR spectra from above (squares), as well as spectra of BS assayed with 400  $\mu\text{M}$  AdoMet (circles, 9.4733 GHz, 10 mW, 20 K), were double integrated after manually subtracting the flavin semiquinone contribution, and the resulting spectra were compared to  $\text{Cu}^{2+}$ –EDTA standards to determine spin concentration.

concentrations (1 equiv per BS dimer), the apparent rate of development of the EPR signal is significantly slowed ( $k_{\text{obs}} \approx 0.02 \text{ min}^{-1}$ ) possibly due to incomplete occupancy of the enzyme active sites with limiting AdoMet.

**Formation of the Reduced FeS Cluster Parallels Production of MDTB.** In parallel with the collection of the EPR samples described above, additional samples were also collected and quenched with acid to denature the protein and release any bound DTB, MDTB, and biotin. The production of MDTB was analyzed by HPLC with UV detection<sup>8</sup> and is compared to the EPR signal intensity (open circles) in Figure 4. We observe that MDTB (filled triangles) forms rapidly ( $k_1 \approx 0.1 \text{ min}^{-1}$ ), as also observed in Figure 2 and previously reported, but decays at a slower rate ( $k_2 \approx 0.02 \text{ min}^{-1}$ ), possibly due to the lower concentration of AdoMet and incubation temperature ( $\sim 25^\circ\text{C}$ ). When compared to the concentration of reduced FeS clusters (open circles), the formation of MDTB parallels FeS cluster reduction, both in magnitude (maximally  $\sim 60 \mu\text{M}$  or  $\sim 0.6$  equiv per dimer) and in the approximate rate of formation and decay. The only notable discrepancy is the apparent steady-state concentration of these putative intermediates,  $\sim 50 \mu\text{M}$  MDTB vs  $\sim 40 \mu\text{M}$  reduced FeS cluster (although this range is within the estimated error of the experiment). In contrast, biotin formation (filled diamonds)

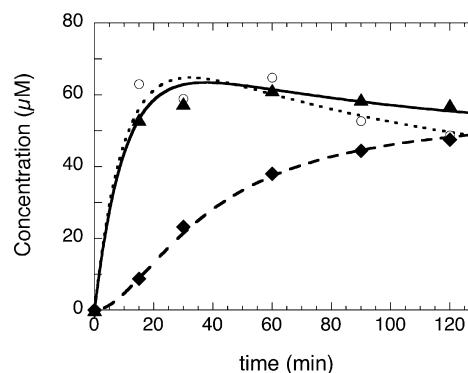


**Figure 4.** Formation and decay of the reduced FeS cluster parallels formation and decay of the reaction intermediate MDTB. BS (100  $\mu\text{M}$  dimer) was incubated with DTB (400  $\mu\text{M}$ ) and AdoMet (400  $\mu\text{M}$ ) at ambient temperature ( $\sim 25^\circ\text{C}$ ) in an anaerobic glovebox, with other components of the assay as described in the Materials and Methods. Samples were collected for EPR analysis, and the FeS cluster spin concentration (circles, dotted curve) was determined as described in Figure 3B. Parallel samples were also collected for HPLC analysis, and the concentration of MDTB (triangles, solid curve) and biotin (diamonds, dashed curve) was determined. The curves represent a fit to a two-step sequential reaction sequence,<sup>8</sup> in which MDTB and the reduced FeS cluster are formed at  $k_1 \approx 0.1 \text{ min}^{-1}$  and then decay at a rate of  $k_2 \approx 0.02 \text{ min}^{-1}$  to steady-state concentration of 40–50  $\mu\text{M}$ . Differences between MDTB and FeS cluster fits are due to small differences in the maximum and steady-state concentrations. Biotin exhibits a short lag followed by a burst ( $k_{\text{burst}} \approx 0.02 \text{ min}^{-1}$ ) and is then formed with  $k_{\text{SS}} \approx 0.002 \text{ min}^{-1}$ .

initially lags behind both MDTB formation and formation of the reduced FeS cluster, consistent with prior studies that demonstrated that MDTB is an intermediate that is transformed into biotin.<sup>8,10,27</sup> Thus, we would suggest that MDTB and the reduced FeS cluster are both catalytic intermediates that are formed at equivalent concentrations in the same reaction step.

It should be noted that this comparison has some associated uncertainty: the concentration of MDTB was determined using biotin as a standard and using an estimate of the extinction coefficient for MDTB based on similar thiol and thioether containing compounds (see Materials and Methods for a more detailed description). In addition, the spin quantitation procedure has an associated uncertainty of ca. 10–20%.

**EPR Spectra Are Simulated by Two Overlapping Rhombic Signals.** The EPR spectrum detected during BS turnover contains multiple components, suggesting an overlap of signals arising from two or more spin systems. To further characterize the spectrum, a sample of BS (100  $\mu\text{M}$  dimer) was prepared as described above, except that the concentration of flavodoxin used in the assay mixture was reduced to 2  $\mu\text{M}$  to minimize the overlapping flavin semiquinone signal. The EPR spectrum was recorded as a function of microwave power, and the spectra were scaled so as to superimpose the high-field region from 340 to 370 mT. As shown in Figures 5A and 6B, the low intensity and narrow flavin contribution is easily saturated relative to the other components. At a power of 100 mW, it is sufficiently saturated such that its contribution to the total spectrum is negligible, and the resulting spectrum (thick solid line in Figure 5A) represents the signal from only the iron–sulfur cluster components. The spectrum has two high-field troughs at  $g = 1.88$  and  $1.85$  that suggest an overlap of two FeS cluster signals and can be simulated as the sum of two

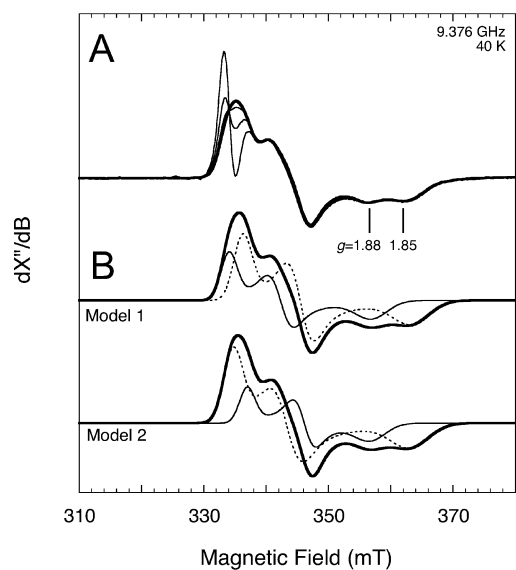


**Figure 5.** EPR spectra of BS frozen during turnover. BS (100  $\mu\text{M}$  dimer) was incubated with DTB (400  $\mu\text{M}$ ), AdoMet (400  $\mu\text{M}$ ), and flavodoxin (2  $\mu\text{M}$ ) for 90 min at 37  $^{\circ}\text{C}$  and then transferred to an EPR tube and frozen in liquid nitrogen. (A) Scaled experimental spectra recorded at 9.376 GHz and 40 K and varying microwave power (thin lines: 0.1, 1, and 10 mW; thick line: 100 mW) show the progressive saturation of the flavin signal at 334 mT and two components of the iron–sulfur signal. (B) Two possible two-component models that accurately fit the 100 mW spectrum (thick solid). Model 1:  $g = [1.9947, 1.9410, 1.8458]$ , 64% (dashed), and  $g = [2.0079, 1.9590, 1.8787]$ , 36% (thin solid). Model 2:  $g = [2.0037, 1.9533, 1.8469]$ , 74% (dashed), and  $g = [1.9906, 1.9375, 1.8796]$ , 26% (thin solid).

rhombohedral  $S = 1/2$  FeS cluster signals. However, the composition and  $g$  tensors of the components can be modeled with two equally accurate sets of parameters (Figure 5B): model 1:  $g = [1.9947, 1.9410, 1.8458]$ , 64% and  $g = [2.0079, 1.9590, 1.8787]$ , 36%, or model 2:  $g = [2.0037, 1.9533, 1.8469]$ , 74%, and  $g = [1.9906, 1.9375, 1.8796]$ , 26%. In model 1, the  $g$  tensors of the two components differ in their mean, but not much in their anisotropy, whereas in model 2, the  $g$  tensors differ in their anisotropy but not their mean. Common to both models is that the component with  $g \approx 1.85$  is the major component (64% and 74%) and the component with  $g \approx 1.88$  is the minor component (36% and 26%). The first set of parameters is similar to those reported by Huynh and co-workers,<sup>16</sup> with similar  $g$  values and only slight differences in the respective ratios of the individual components. Of particular interest, both studies report that two overlapping signals are formed in parallel following incubation under assay conditions, and we further have observed that the ratio of these two signals does not change as the signals grow and decay over time (Figure 3A) or as the sample temperature is altered (Figure 6A). It might be conceivable that, instead of two components, the spectrum consists of only one  $S = 1/2$  component with the two high-field troughs resulting from hyperfine splitting due to a proton, possibly from the Arg260 ligand. However, we were not able to accurately fit the spectrum with this assumption; specifically, hyperfine splitting by a proton would have generated a spectrum in which the trough at  $g \approx 1.88$  is deeper than the trough at  $g \approx 1.85$ .

The observed EPR spectra are not similar to spectrum of the  $[2\text{Fe}-2\text{S}]^+$  cluster observed by Lotierzo et al. in the chemically reduced Asn153Ala mutant enzyme.<sup>23</sup> The  $[2\text{Fe}-2\text{S}]^+$  cluster

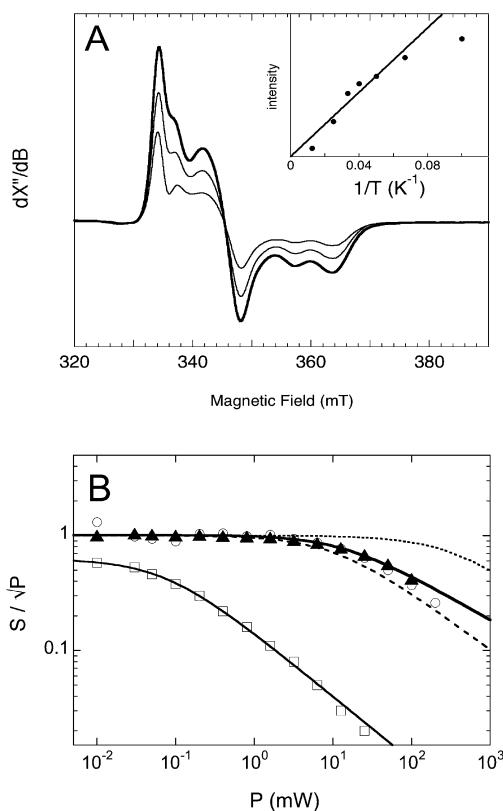


**Figure 6.** Temperature and microwave power dependence of EPR spectra of BS (100  $\mu\text{M}$  dimer) incubated with DTB (400  $\mu\text{M}$ ) and AdoMet (400  $\mu\text{M}$ ) for 60 min at 25  $^{\circ}\text{C}$ , with other assay conditions as described in the Materials and Methods. (A) Spectra were recorded at varying sample temperatures (10–80 K), with the microwave power held constant at 1 mW, and the total integrated intensity of the absorption spectrum is plotted vs inverse temperature, showing approximate Curie law dependence (inset). Spectra are shown for 15 (thick curve), 25, and 40 K. (B) Spectra recorded at varying microwave power (0.01–150 mW), with the sample temperature held constant at 20 K, and the intensity of the signal at 348 mT divided by the square root of the microwave power ( $\blacktriangle$ ) is plotted vs power. Similar data were collected for the Arg260Met mutant ( $\circ$ ) and flavodoxin FMN semiquinone ( $\square$ ). Data are fit to power saturation curves using  $P_{1/2} = 19$  mW for BS and  $P_{1/2} = 0.07$  mW for flavodoxin (solid curves). Simulated power saturation curves at 20 K for the *H. halobium* ferredoxin  $[2\text{Fe}-2\text{S}]^+$  cluster ( $P_{1/2} = 10$  mW, dashed curve) and the *B. stearothermophilus* ferredoxin  $[4\text{Fe}-4\text{S}]^+$  cluster ( $P_{1/2} = 330$  mW, dotted curve) are shown for reference.<sup>29</sup>

produced by chemical reduction exhibits an axial spectrum with  $g_{\perp} \approx 2.00$  and  $g_{\parallel} \approx 1.91$ , while the reduced cluster observed during enzyme turnover exhibits a rhombic spectrum with  $g_{x,y,z} \approx [2.00, 1.95, 1.85]$  for the major component as described above. Minimally, the dissimilarity of the spectra observed following chemical reduction vs enzyme turnover suggests that the paramagnetic cluster generated during turnover does not correspond to simple reduction of the  $[2\text{Fe}-2\text{S}]^+$  cluster by electron transfer. The increased dispersion of  $g$  tensors during catalytic turnover could result from decreased structural symmetry, as might be expected if MDTB coordinates to and distorts the  $[2\text{Fe}-2\text{S}]^+$  cluster.

**Relaxation Properties of the EPR Signals Are Consistent with a  $[2\text{Fe}-2\text{S}]^+$  Cluster.** The line shape and  $g$  values associated with the observed EPR signal are consistent with either  $[2\text{Fe}-2\text{S}]^+$  or  $[4\text{Fe}-4\text{S}]^+$  clusters. Since the initial

active BS sample contains both  $[2\text{Fe}-2\text{S}]^{2+}$  and  $[4\text{Fe}-4\text{S}]^{2+}$  clusters,<sup>18,28</sup> electron transfer during formation of MDTB could lead to reduction of one or both clusters. To distinguish both the number and type of reduced FeS clusters, we probed the spin relaxation properties of the cluster by examining the signal intensity as a function of both sample temperature and microwave power. Samples of WT BS and the active Arg260Met mutant (100  $\mu\text{M}$  dimer) were prepared by incubating with DTB (400  $\mu\text{M}$ ) and AdoMet (400  $\mu\text{M}$ ) for 90 min, in a similar manner as described above. The sample temperature was varied (10–80 K) at a constant moderate microwave power (1 mW), and the most intense spectra were observed at 15–20 K (Figure 6A). The decrease in signal intensity was as predicted by the Curie law (Figure 6A inset) except at very low temperature (10 K), where partial signal saturation was observed due to the moderately high microwave power. The microwave power was then varied (0.01–200 mW) at a constant sample temperature (20 K), and EPR spectra show that the signal observed in both the WT and Arg260Met BS is only partially saturated at moderate-to-high power ( $P_{1/2} = 19$  mW, Figure 6B). For comparison, the  $[2\text{Fe}-2\text{S}]^+$  cluster of *Halobacterium halobium* ferredoxin exhibits a maximum signal at 20–40 K and is saturated at a similar moderate power ( $P_{1/2} = 10$  mW, Figure 6B, dashed curve).<sup>29</sup> In contrast,  $[4\text{Fe}-4\text{S}]^+$  clusters typically are very fast relaxing and show saturation only at very high microwave powers (>50 mW) and very low temperatures (<10 K). For example, the  $[4\text{Fe}-4\text{S}]^+$  cluster in *B. stearothermophilus* ferredoxin has a half-saturation power of  $P_{1/2} = 330$  mW (Figure 6B, dotted curve).<sup>29</sup> In contrast, the isotropic signal at  $g = 2.005$  arising from the flavin semiquinone is easily saturated at very low power ( $P_{1/2} = 0.07$  mW).

Johnson and co-workers have noted that the dithionite-reduced  $[4\text{Fe}-4\text{S}]^+$  cluster in BS has intermediate relaxation properties and is also partially saturated above 10 mW at 20 K.<sup>20</sup> However, the  $[4\text{Fe}-4\text{S}]^+$  cluster spectrum exhibits  $g$  values of 2.044, 1.944, and 1.914<sup>20</sup> that are significantly higher than those reported in this study. Therefore, on the basis of spin relaxation properties and  $g$  values, the signal we observe during BS turnover can be most likely attributed to a somewhat fast-relaxing  $[2\text{Fe}-2\text{S}]^+$  cluster. As noted previously, Jameson et al. have characterized a similar EPR-detectable signal as a minor component of the total cluster content of BS incubated with substrates and have attributed the signal to a  $[2\text{Fe}-2\text{S}]^+$  cluster on the basis of Mössbauer parameters.<sup>16</sup> It should also be noted that the major features of the complex EPR signal respond to changes in sample temperature and microwave power in a similar manner, suggesting that these have identical spin relaxation properties and arise from the same type of FeS cluster within the enzyme.

**Arg260Met Mutation Alters the  $g$  Tensors in the EPR Spectrum.** Arginine is an unusual metal ligand,<sup>30</sup> particularly for an FeS cluster, yet in BS it is a highly conserved residue that is coordinated to via the guanidino group to the  $[2\text{Fe}-2\text{S}]$  cluster.<sup>12</sup> In a previous study, we demonstrated that the enzyme retains nearly full catalytic activity when Arg260 is replaced by several other amino acid residues, including alanine, histidine, and methionine (but not cysteine).<sup>31</sup> Replacement of arginine by alanine may leave a pocket in the active site that allows coordination of water to the  $[2\text{Fe}-2\text{S}]^{2+}$  cluster in place of arginine, while histidine and methionine side chains are predicted to be sufficiently long that they can coordinate directly to the  $[2\text{Fe}-2\text{S}]^{2+}$  cluster. Consistent with this hypothesis, there is a significant change in the UV/vis spectrum

of the  $[2\text{Fe}-2\text{S}]^{2+}$  cluster in the Arg260Met mutant as compared to WT (Figure 7A), suggesting changes in the relative energies of ligand-to-metal charge-transfer bands.

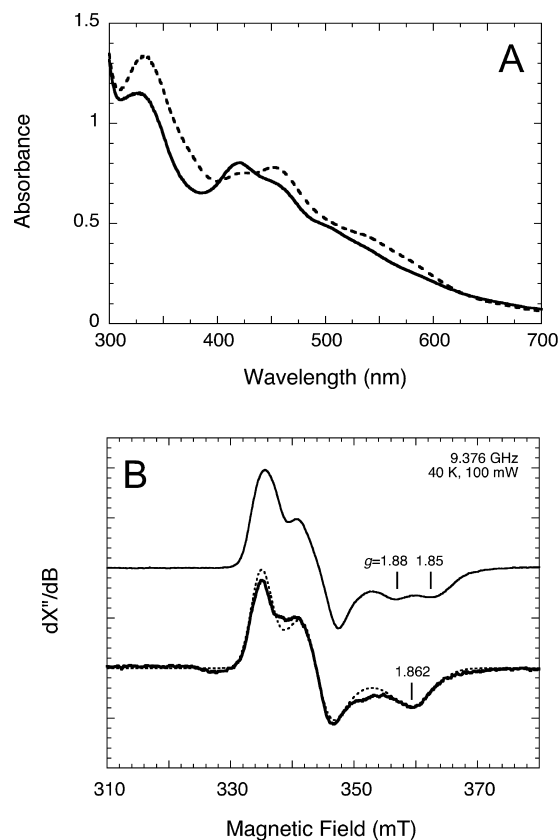


**Figure 7.** Arg260Met mutant enzyme exhibits altered spectroscopic properties for the reduced FeS cluster. (A) UV/vis spectra of WT (dashed curve) and Arg260Met BS (solid curve, 50  $\mu\text{M}$  dimer) aerobically purified containing one  $[2\text{Fe}-2\text{S}]^{2+}$  cluster per monomer. Shifts in the position and intensity of the major ligand-to-metal charge transfer bands in the UV/vis spectrum suggest that the methionine sulfur atom replaces the arginine nitrogen atom as a ligand to the  $[2\text{Fe}-2\text{S}]^{2+}$  cluster. (B) EPR spectra of the  $[2\text{Fe}-2\text{S}]^+$  clusters in WT and Arg260Met mutant enzymes (100  $\mu\text{M}$  dimer), experimental (solid) and simulated (dashed). Aliquots were incubated with DTB (400  $\mu\text{M}$ ) and AdoMet (400  $\mu\text{M}$ ) for 90 min, with other assay conditions as described in the Materials and Methods. Samples were frozen in liquid  $\text{N}_2$ , and EPR spectra were collected at 9.376 GHz, 100 mW, 40 K. Simulation parameters for the EPR spectrum of the Arg260Met mutant enzyme:  $g = [2.000, 1.947, 1.862]$ .

Since Arg260 is coordinated to the  $[2\text{Fe}-2\text{S}]^{2+}$  cluster, changes in the EPR spectrum of the Arg260Met mutant are expected if the spectrum is due to the  $[2\text{Fe}-2\text{S}]^+$  cluster. The Arg260Met mutant enzyme was incubated with DTB and AdoMet under assay conditions for 90 min, as described above for the WT enzyme, and a sample frozen in liquid  $\text{N}_2$ . Similar to WT enzyme, the EPR spectrum of the Arg260Met enzyme was recorded under conditions (40 K, 100 mW) that saturate the flavin semiquinone radical and minimize the contribution of this signal to the EPR spectra. In contrast to the WT enzyme, the EPR spectrum of the Arg260Met mutant enzyme shows only a single  $S = 1/2$  component with a rhombic  $g$  tensor. The high-field component at  $g \approx 1.862$  falls directly between the two high-field components of the WT enzyme spectrum. The other  $g$  tensor values are not significantly different from the

values obtained from simulations of the WT enzyme. The observation of a significant change in the high-field  $g$  tensor upon mutation of a coordinating ligand supports the assignment of the EPR signal to a reduced state of the  $[2\text{Fe}-2\text{S}]$  cluster.

### Coupling of the Unpaired Electron to Nitrogen Is Observed in WT BS, but Not in the Arg260Met Mutant.

Typical FeS clusters in nonisotopically labeled proteins exhibit small hyperfine coupling to nearby hydrogen atoms ( $^1\text{H}$ ) bonded to the FeS cluster ligands (e.g., cysteine  $\text{H}_\beta$ ) and to nitrogen atoms ( $^{14}\text{N}$ ) in nearby functional groups. Weak  $^{14}\text{N}$  coupling has been attributed to through-space coupling to nearby amide nitrogen atoms, while strong  $^{14}\text{N}$  coupling implies a close proximity that is only achieved by covalent coordination of a nitrogen-containing amino acid ligand to the FeS cluster. ESEEM is a pulsed EPR technique that allows detection of hyperfine coupling of unpaired electrons to nearby nuclear spins.<sup>32</sup> Since WT BS contains a single arginine ligand to the  $[2\text{Fe}-2\text{S}]^{2+}$  cluster that is eliminated in the Arg260Met mutant, ESEEM spectra should provide additional confirmation that the EPR spin is localized on the  $[2\text{Fe}-2\text{S}]$  cluster. Three-pulse X-band ESEEM spectra were recorded at several magnetic field positions across the EPR spectrum of WT enzyme (Figure 8, solid curves), and the spectra show peaks

space coupling to the Cys97, Cys128, or Cys188 amide nitrogen atoms (5–6 Å Fe–N distance) or the nearby Arg95 side chain (5–7 Å Fe–N distance).

The ESEEM spectra in Figure 8 show three sharp peaks at 0.5, 1.6–1.8, and 2.3–2.4 MHz due to  $^{14}\text{N}$  in the cancellation regime.<sup>33</sup> We can estimate the  $^{14}\text{N}$  quadrupole parameters from these frequencies and get  $|K| = |e^2Qq/4h| \approx 0.65\text{--}0.70$  MHz and  $\eta \approx 0.36\text{--}0.54$ . Histidine can be excluded as a source of these signals, as the closest one (His152) is  $>10$  Å away from the  $[2\text{Fe}-2\text{S}]$  cluster. The value of  $|K|$  is inconsistent with a primary aliphatic amine ( $|K| \approx 1$  MHz),<sup>34</sup> and it is lower than the values observed for backbone amide nitrogens in peptides ( $|K| \approx 0.75\text{--}0.85$  MHz).<sup>35,36</sup> The values fall in the range of those assigned to Arg side chains in nitrogenase ( $|K| \approx 0.54$  MHz,  $\eta \approx 0.59$ )<sup>37</sup> and ethanolamine ammonia-lyase ( $|K| \approx 0.76$  MHz,  $\eta \approx 0.55$ ).<sup>38</sup> Therefore, the  $^{14}\text{N}$  peaks in Figure 8 are consistent with an assignment to Arg260. In addition, the fact that the weak ESEEM peaks in the Arg260Met mutant are at similar frequencies than in the WT supports arginine assignments in both variants (Arg260 in the WT and Arg95 in the mutant). However, further study is required to confirm this and to identify the particular  $^{14}\text{N}$  in the Arg260 side chain that is responsible for the ESEEM modulations.

## DISCUSSION

The chemical properties and biochemical function of the iron–sulfur clusters in BS have been the subject of numerous investigations (reviewed in ref 1). When aerobically purified, recombinant BS contains a  $[2\text{Fe}-2\text{S}]^{2+}$  cluster<sup>19</sup> that is also observed as the primary cofactor component *in vivo* using whole-cell Mössbauer spectroscopy.<sup>39,40</sup> In addition, a  $[4\text{Fe}-4\text{S}]^{2+/+}$  cluster can be chemically reconstituted by incubation with  $\text{Fe}^{2+/3+}$ ,  $\text{S}^{2-}$ , and a chemical reductant.<sup>18,41,42</sup> On the basis of spectroelectrochemical titrations<sup>18</sup> and Mössbauer spectroscopy of differentially reconstituted  $^{57}\text{Fe}$  protein,<sup>28</sup> the  $[2\text{Fe}-2\text{S}]^{2+}$  and  $[4\text{Fe}-4\text{S}]^{2+/+}$  clusters were found to occupy different sites within the protein, a feature later confirmed by the X-ray crystal structure of the reconstituted protein with substrates bound.<sup>12</sup> Most importantly, only protein that contains both the  $[2\text{Fe}-2\text{S}]^{2+}$  cluster and the  $[4\text{Fe}-4\text{S}]^{2+}$  cluster is significantly active *in vitro*.<sup>15</sup>

The chemical properties the  $[2\text{Fe}-2\text{S}]^{2+}$  cluster and the role of this cluster in biotin formation have remained somewhat controversial. The X-ray crystal structure shows that this cluster is bound to Cys97, Cys121, Cys188, and Arg260 and resides  $\sim 4.6$  Å away from DTB. The proximity of the  $[2\text{Fe}-2\text{S}]^{2+}$  cluster to DTB has led us to suggest that this cluster plays a role in sulfur insertion.<sup>12,15</sup> Several studies have examined the fate of the  $[2\text{Fe}-2\text{S}]^{2+}$  cluster under *in vitro* assay conditions. Using UV/vis spectra of reconstituted BS, we have shown that at least a portion of the  $[2\text{Fe}-2\text{S}]^{2+}$  cluster is reduced or lost at a rate that is similar to the rate of biotin formation.<sup>15</sup> Marquet and co-workers subsequently examined the transformation of the FeS clusters in partially purified  $^{57}\text{Fe}$ -labeled BS using Mössbauer spectroscopy.<sup>43</sup> Prior to the addition of substrates, the Mössbauer spectrum of the initial protein is best modeled by an approximate 1:1 ( $\pm 0.1$ ) ratio of  $[2\text{Fe}-2\text{S}]^{2+}$  and  $[4\text{Fe}-4\text{S}]^{2+}$  clusters. While incubation with DTB alone did not affect the ratio of FeS clusters, incubation with both DTB and AdoMet decreased the  $[2\text{Fe}-2\text{S}]^{2+}$  to  $[4\text{Fe}-4\text{S}]^{2+}$  cluster ratio to 0.6:1, while simultaneously increasing the concentration of high-spin  $\text{Fe}^{3+}$  species, most likely in the buffer.<sup>43</sup> Huynh and co-workers undertook a more detailed analysis of changes in the  $[2\text{Fe}-$

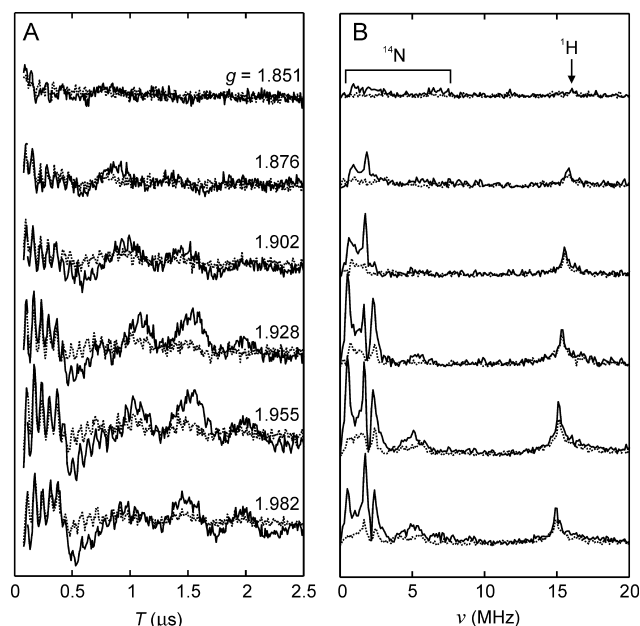


**Figure 8.** Comparison of ESEEM spectra of WT and Arg260Met mutant enzymes. (A) Three-pulse ESEEM decay envelopes with  $\tau = 160$  ns measured at 10 K, 9.71 GHz, and magnetic field strengths corresponding to  $g$  values of 1.851, 1.876, 1.902, 1.928, 1.955, and 1.982. WT (solid) and Arg260Met (dotted). (B) Peaks corresponding to electron–nuclear coupling to  $^1\text{H}$  appear at around 15 MHz and are present in both WT (solid) and Arg260Met (dotted), but peaks corresponding to electron–nuclear coupling to  $^{14}\text{N}$  appear at 2–6 MHz only for WT BS with the Arg260 ligand to the  $[2\text{Fe}-2\text{S}]^{2+}$  cluster and are largely lost in spectra of the Arg260Met mutant, which contains only sulfur ligands to the  $[2\text{Fe}-2\text{S}]^{2+}$  cluster.

due to coupling to  $^1\text{H}$  nuclei at 15 and 30 MHz and peaks due to coupling to  $^{14}\text{N}$  nuclei at 2–6 MHz. In contrast, ESEEM spectra of the Arg260Met mutant enzyme measured under the same conditions (Figure 8, dotted curves) have only very weak intensity in the 1–6 MHz region, most likely due to through-

$2S]^{2+}$  cluster during enzyme turnover by combining EPR and Mössbauer spectroscopy of BS that was  $^{57}\text{Fe}$ -labeled in only the  $[2\text{Fe}-2S]^{2+}$  cluster.<sup>16</sup> They also report a significant decrease in the concentration of the  $[2\text{Fe}-2S]^{2+}$  cluster and report the transient formation of a  $[2\text{Fe}-2S]^+$  cluster followed by an increase in the concentration of high-spin  $\text{Fe}^{2+}$ . Although in principle these reports are consistent with the involvement of the  $[2\text{Fe}-2S]^{2+}$  cluster in providing sulfur for biotin formation, Huynh and co-workers noted a significant discrepancy between the rate of  $[2\text{Fe}-2S]^{2+}$  cluster degradation ( $0.13 \text{ min}^{-1}$ ) and the rate of biotin formation ( $0.012 \text{ min}^{-1}$ ). They suggested that an alternative mechanism in which the cluster degrades to provide a persulfide sulfur for biotin formation could not be ruled out.

In the present work, we show that reduction of the  $[2\text{Fe}-2S]^{2+}$  cluster to a  $[2\text{Fe}-2S]^+$  cluster is kinetically correlated with the production of MDTB, with an approximate 1:1 stoichiometric ratio (Figure 4). However, given the experimental uncertainties involved, and the relatively slow progress of both MDTB and biotin formation, we cannot necessarily distinguish whether reduction of the  $[2\text{Fe}-2S]^{2+}$  cluster occurs in the same chemical step as MDTB formation or occurs immediately prior to or after C-S bond formation. However, since a reduced  $[2\text{Fe}-2S]^+$  cluster is never observed in the absence of DTB, despite the presence of the complete flavodoxin reducing system, we conclude that it is DTB, or more specifically, the quenching of the DTB carbon radical that triggers reduction of this cluster.<sup>8</sup>

The apparent complexity of the resulting EPR spectrum is due to the overlap of two rhombic EPR signals, both of which are fairly typical of reduced FeS clusters. The same  $\sim 2:1$  ratio of signals has now been observed in two different laboratories with different preparations of enzyme. The ratio of these two signals is also not sensitive to incubation time, sample temperature, or microwave power, suggesting the two signals arise simultaneously in the assay and have nearly identical spin relaxation properties. The origin of the two overlapping signals is not presently understood. One possible explanation for the occurrence of two components is differential valence localization on the two iron atoms within the  $[2\text{Fe}-2S]^+$  cluster. The electronic state of the reduced cluster can be described as a high-spin  $\text{Fe}^{2+}$  site ( $S = 2$ ) antiferromagnetically coupled to a high-spin  $\text{Fe}^{3+}$  site ( $S = 5/2$ ). If there is a preference for  $\text{Fe}^{2+}$  to reside at one site over the other, as for example has been observed in Rieske-type  $[2\text{Fe}-2S]^+$  proteins with  $\text{Fe}^{2+}$  coordinated by two His residues and  $\text{Fe}^{3+}$  coordinated by two Cys residues, then the unpaired electron spin is not delocalized over the entire cluster.<sup>44</sup> In our system, there could be only a small energy difference between the two electronic states ( $2:1$  ratio corresponds to  $\sim 0.1 \text{ kJ}$  at  $20 \text{ K}$ ), such that both possible spin valence-localized states are occupied in different FeS clusters within the frozen sample. A more detailed analysis of hyperfine coupling constants that arise from coupling of the electron spin to  $^{14}\text{N}/^{15}\text{N}$  of Arg260 using ESEEM and ENDOR spectroscopy would provide a more complete electronic description of the reduced cluster.

An alternative explanation for the observation of two distinct EPR signals could be structural heterogeneity within the active site of the intermediate. For example, the MDTB thiolate could equilibrate between coordination to the two opposing Fe atoms within the intermediate cluster. However, assuming that the general scheme depicted in Figure 1A is correct, then the quenching of a DTB carbon radical by the  $\mu$ -sulfide of the

$[2\text{Fe}-2S]^{2+}$  cluster would initially generate a reduced cluster in which the MDTB thiolate is a symmetric bridging ligand. This cluster would be best described as a  $[\text{Fe}_2(\mu\text{-S})(\mu\text{-S-MDTB})(\text{S-Cys})_3(\text{NH}_2\text{-Arg})]^-$  cluster. A somewhat similar synthetic cluster,  $[\text{Fe}_2(\mu\text{-S})(\mu\text{-S-Et})(\text{NO})_4]^-$ , was recently characterized by various spectroscopic methods and by high-resolution X-ray crystallography, and the core was described as a slightly nonplanar rhombus (dihedral angle =  $171.7^\circ$ ) with equivalent bond distances between the Fe atoms and the bridging  $\text{EtS}^-$  ligand.<sup>45</sup> This cluster had physical properties that were only slightly altered from the values for the corresponding  $[\text{Fe}_2(\mu\text{-S})_2(\text{NO})_4]^{2-}$  cluster and in most respects behaved in a manner that would be indistinguishable from a typical FeS cluster. On the basis of this chemical precedent, we would predict that structure of the BS intermediate FeS cluster likely includes a symmetric bridging MDTB thiolate ligand (Figure 1A). From a cursory examination of the initial active site structure, containing AdoMet, DTB, and the  $[2\text{Fe}-2S]^{2+}$  cluster (Figure 1B), it appears that repositioning of MDTB as a symmetric bridging thiolate ligand would require significant reorganization of the active site and that the current structural data may not be sufficient to describe this intermediate or the subsequent ring-closing reaction.

Another possible origin of structural heterogeneity, and consequently a possible reason for the two spectral components, could be the positioning of the arginine ligand relative to the  $[2\text{Fe}-2S]^+$  cluster. The guanidine group has two terminal nitrogen atoms that could coordinate the iron. From the X-ray crystal structure, Fe-N<sub>o</sub> distances of 2.35 and 3.15 Å were found, but it is possible that this geometry rearranges upon reaction of DTB with the bridging sulfur and concomitant changes in the geometry of the FeS cluster core. Lastly, the two spectral components could possibly arise from two different protonation states of the guanidine group of Arg260. Clearly, a more precise structural and electronic description of the intermediate state will be required to distinguish between these various hypotheses.

Several AdoMet radical enzymes have now been identified that catalyze the formation of new carbon-sulfur bonds using FeS clusters as the probable source of sulfur atoms. *E. coli* lipoyl synthase (LipA) catalyzes the addition of two sulfur atoms to octanoyl-E2 protein or octanoyl-H protein to generate lipoyl-protein, with both sulfur atoms most likely derived from a  $[4\text{Fe}-4\text{S}]$  cluster within a single enzyme monomer.<sup>46-48</sup> *S. solfataricus* LipA will accept a octanoyl-tripeptide substrate and generates a C6 monothiolated intermediate prior to addition of the second sulfur atom.<sup>49</sup> *T. maritima* MiaB catalyzes the methylthiolation at the C2 position of (N6-isopentenyl)-adenosine-37 in certain tRNAs, with the sulfur atom possibly derived from a  $[4\text{Fe}-4\text{S}]$  cluster.<sup>50</sup> RimO catalyzes the methylthiolation of an aspartate residue in the ribosomal protein S12, and the presence of two  $[4\text{Fe}-4\text{S}]$  clusters in the enzyme again suggests the sulfur atom is derived from one of these clusters.<sup>51</sup> Presumably these sulfur insertion reactions will share some features of the biotin synthase reaction mechanism. In particular, formation of a carbon-sulfur bond by attack of a carbon radical on sulfide must be accompanied by one electron oxidation of the sulfur atom, and presumably this would be accompanied by transfer of this electron into the FeS cluster. In most cases, these other enzymes have been assayed in the presence of excess dithionite, resulting in an equilibrium concentration of chemically reduced FeS clusters that obscures observation of paramagnetic enzyme intermediates and may

also inhibit enzyme activity. If assay conditions could be developed with enzyme initially containing only diamagnetic  $[4\text{Fe}-4\text{S}]^{2+}$  clusters, and in which the natural reducing system supports AdoMet radical generation, then we would predict that paramagnetic  $[4\text{Fe}-4\text{S}]^+$  clusters would be generated during catalysis, either as an intermediate in LipA or as an enzyme-bound product in MiaB or RimO.

## AUTHOR INFORMATION

### Corresponding Author

\*Phone: 808-956-6721. Fax: 808-956-5908. E-mail: jtj@hawaii.edu.

### Funding

This research has been supported by grants from the NSF (MCB 09-23829 to J.T.J.) and the NIH (GM73789 to R.D.B.).

## ACKNOWLEDGMENTS

We thank Dr. Christine Farrar for supplying data incorporated into Figure 2 and Corey Fugate for supplying data incorporated into Figure 6.

## ABBREVIATIONS

AdoMet, S-adenosyl-L-methionine; BS, biotin synthase; dAH, 5'-deoxyadenosine;  $\text{dA}^\bullet$ , 5'-deoxyadenosyl radical; DTB, dethiobiotin; DTT, dithiothreitol; EPR, electron paramagnetic resonance; ESEEM, electron spin echo envelope modulation; Fld, flavodoxin; FNR, ferredoxin (flavodoxin): NADP<sup>+</sup> oxidoreductase; MDTB, 9-mercaptodethiobiotin; Tris, tris-(hydroxymethyl)aminomethane.

## REFERENCES

- Jarrett, J. T. (2005) The novel structure and chemistry of iron-sulfur clusters in the adenosylmethionine-dependent radical enzyme biotin synthase. *Arch. Biochem. Biophys.* 433, 312–321.
- Marquet, A. (2001) Enzymology of carbon-sulfur bond formation. *Curr. Opin. Chem. Biol.* 5, 541–549.
- Marquet, A., Florentin, D., Ploux, O., and Tse Sum Bui, B. (1998) In vivo formation of C-S bonds in biotin. An example of radical chemistry under reducing conditions. *J. Phys. Org. Chem.* 11, 529–535.
- Escalletes, F., Florentin, D., Tse Sum Bui, B., Lesage, D., and Marquet, A. (1999) Biotin Synthase Mechanism: Evidence for Hydrogen Transfer from the Substrate into Deoxyadenosine. *J. Am. Chem. Soc.* 121, 3571–3578.
- Gibson, K. J., Pelletier, D. A., and Turner, I. M. Sr. (1999) Transfer of sulfur to biotin from biotin synthase (BioB protein). *Biochem. Biophys. Res. Commun.* 254, 632–635.
- Tse Sum Bui, B., Florentin, D., Fournier, F., Ploux, O., Mejean, A., and Marquet, A. (1998) Biotin synthase mechanism: on the origin of sulphur. *FEBS Lett.* 440, 226–230.
- Tse Sum Bui, B., Mattioli, T. A., Florentin, D., Bolbach, G., and Marquet, A. (2006) *Escherichia coli* biotin synthase produces selenobiotin. Further evidence of the involvement of the  $[2\text{Fe}-2\text{S}]^{2+}$  cluster in the sulfur insertion step. *Biochemistry* 45, 3824–3834.
- Taylor, A. M., Farrar, C. E., and Jarrett, J. T. (2008) 9-Mercaptodethiobiotin is formed as a competent catalytic intermediate by *Escherichia coli* biotin synthase. *Biochemistry* 47, 9309–9317.
- Guianvarc'h, D., Florentin, D., Tse Sum Bui, B., Nunzi, F., and Marquet, A. (1997) Biotin synthase, a new member of the family of enzymes which uses S-adenosylmethionine as a source of deoxyadenosyl radical. *Biochem. Biophys. Res. Commun.* 236, 402–406.
- Shaw, N. M., Birch, O. M., Tinschert, A., Venetz, V., Dietrich, R., and Savoy, L. A. (1998) Biotin synthase from *Escherichia coli*: isolation of an enzyme-generated intermediate and stoichiometry of S-adenosylmethionine use. *Biochem. J.* 330, 1079–1085.
- Farrar, C. E., and Jarrett, J. T. (2007) Radical S-Adenosylmethionine (SAM) Superfamily, in *Encyclopedia of the Life Sciences*, John Wiley & Sons, Ltd., Chichester.
- Berkovitch, F., Nicolet, Y., Wan, J. T., Jarrett, J. T., and Drennan, C. L. (2004) Crystal structure of biotin synthase, an S-adenosylmethionine-dependent radical enzyme. *Science* 303, 76–79.
- Cosper, M. M., Jameson, G. N., Davydov, R., Eidsness, M. K., Hoffman, B. M., Huynh, B. H., and Johnson, M. K. (2002) The  $[4\text{Fe}-4\text{S}]^{2+}$  cluster in reconstituted biotin synthase binds S-adenosyl-L-methionine. *J. Am. Chem. Soc.* 124, 14006–14007.
- Hewitson, K. S., Ollagnier-de Choudens, S., Sanakis, Y., Shaw, N. M., Baldwin, J. E., Munck, E., Roach, P., and Fontecave, M. (2002) The iron-sulfur center of biotin synthase: site-directed mutants. *J. Biol. Inorg. Chem.* 7, 83–93.
- Ugulava, N. B., Sacanell, C. J., and Jarrett, J. T. (2001) Spectroscopic changes during a single turnover of biotin synthase: destruction of a  $[2\text{Fe}-2\text{S}]$  cluster accompanies sulfur insertion. *Biochemistry* 40, 8352–8358.
- Jameson, G. N., Cosper, M. M., Hernandez, H. L., Johnson, M. K., and Huynh, B. H. (2004) Role of the  $[2\text{Fe}-2\text{S}]$  cluster in recombinant *Escherichia coli* biotin synthase. *Biochemistry* 43, 2022–2031.
- Jarrett, J. T., and Wan, J. T. (2002) Thermal inactivation of reduced ferredoxin (flavodoxin):NADP<sup>+</sup> oxidoreductase from *Escherichia coli*. *FEBS Lett.* 529, 237–242.
- Ugulava, N.B., Gibney, B. R., and Jarrett, J. T. (2001) Biotin synthase contains two distinct iron-sulfur cluster binding sites: chemical and spectroelectrochemical analysis of iron-sulfur cluster interconversions. *Biochemistry* 40, 8343–8351.
- Sanyal, I., Cohen, G., and Flint, D. H. (1994) Biotin synthase: purification, characterization as a  $[2\text{Fe}-2\text{S}]$  cluster protein, and in vitro activity of the *Escherichia coli* bioB gene product. *Biochemistry* 33, 3625–3631.
- Duin, E. C., Lafferty, M. E., Crouse, B. R., Allen, R. M., Sanyal, I., Flint, D. H., and Johnson, M. K. (1997)  $[2\text{Fe}-2\text{S}]$  to  $[4\text{Fe}-4\text{S}]$  Cluster Conversion in *Escherichia coli* Biotin Synthase. *Biochemistry* 36, 11811–11820.
- Ugulava, N. B., Gibney, B. R., and Jarrett, J. T. (2000) Iron-sulfur cluster interconversions in biotin synthase: dissociation and reassociation of iron during conversion of  $[2\text{Fe}-2\text{S}]$  to  $[4\text{Fe}-4\text{S}]$  clusters. *Biochemistry* 39, 5206–5214.
- Cosper, M.M., Jameson, G. N., Hernandez, H. L., Krebs, C., Huynh, B. H., and Johnson, M. K. (2004) Characterization of the cofactor composition of *Escherichia coli* biotin synthase. *Biochemistry* 43, 2007–2021.
- Lotierzo, M., Bui, B. T., Leech, H. K., Warren, M. J., Marquet, A., and Rigby, S. E. (2009) Iron-sulfur cluster dynamics in biotin synthase: a new  $[2\text{Fe}-2\text{S}](1+)$  cluster. *Biochem. Biophys. Res. Commun.* 381, 487–490.
- Farrar, C.E., Siu, K. K. W., Howell, P. L., and Jarrett, J. T. (2010) Biotin Synthase Exhibits Burst Kinetics and Multiple Turnovers in the Absence of Inhibition by Products and Product-Related Biomolecules. *Biochemistry* 49, 9985–9996.
- Farrar, C.E., and Jarrett, J. T. (2009) Protein residues that control the reaction trajectory in S-adenosylmethionine radical enzymes: mutagenesis of asparagine 153 and aspartate 155 in *Escherichia coli* biotin synthase. *Biochemistry* 48, 2448–2458.
- Wan, J. T., and Jarrett, J. T. (2002) Electron acceptor specificity of ferredoxin (flavodoxin):NADP<sup>+</sup> oxidoreductase from *Escherichia coli*. *Arch. Biochem. Biophys.* 406, 116–126.
- Tse Sum Bui, B., Lotierzo, M., Escalletes, F., Florentin, D., and Marquet, A. (2004) Further investigation on the turnover of *Escherichia coli* biotin synthase with dethiobiotin and 9-mercaptodethiobiotin as substrates. *Biochemistry* 43, 16432–16441.
- Ugulava, N. B., Surerus, K. K., and Jarrett, J. T. (2002) Evidence from Mössbauer spectroscopy for distinct  $[2\text{Fe}-2\text{S}]^{2+}$  and  $[4\text{Fe}-4\text{S}]^{2+}$  cluster binding sites in biotin synthase from *Escherichia coli*. *J. Am. Chem. Soc.* 124, 9050–9051.

- (29) Rupp, H., Rao, K. K., Hall, D. O., and Cammack, R. (1978) Electron spin relaxation of iron-sulphur proteins studied by microwave power saturation. *Biochim. Biophys. Acta* 537, 255–260.
- (30) Di Costanzo, L., Flores, L. V. Jr., and Christianson, D. W. (2006) Stereochemistry of guanidine-metal interactions: implications for L-arginine-metal interactions in protein structure and function. *Proteins* 65, 637–642.
- (31) Broach, R.B., and Jarrett, J. T. (2006) Role of the  $[2\text{Fe-2S}]^{2+}$  cluster in biotin synthase: mutagenesis of the atypical metal ligand arginine 260. *Biochemistry* 45, 14166–14174.
- (32) Chasteen, N. D., and Snetsinger, P. A. (2000) ESEEM and ENDOR Spectroscopy, in *Physical Methods in Bioinorganic Chemistry: Spectroscopy and Magnetism* (Que, L., Jr., Ed.), pp 187–231, University Science Books, Sausalito, CA.
- (33) Flanagan, H.L., and Singel, D. J. (1987) Analysis of  $^{14}\text{N}$  ESEEM patterns of randomly oriented solids. *J. Chem. Phys.* 87, 5606–5616.
- (34) Dikanov, S. A., and Tsvetkov, Y. D. (1992) *Electron Spin Echo Envelope Modulation (ESEEM) Spectroscopy*, CRC Press, Inc., Boca Raton, FL.
- (35) McCracken, J., Vassiliev, I. R., Yang, E. C., Range, K., and Barry, B. A. (2007) ESEEM studies of peptide nitrogen hyperfine coupling in tyrosyl radicals and model peptides. *J. Phys. Chem. B* 111, 6586–6592.
- (36) Yap, L. L., Samoilova, R. I., Gennis, R. B., and Dikanov, S. A. (2006) Characterization of the exchangeable protons in the immediate vicinity of the semiquinone radical at the QH site of the cytochrome bo3 from *Escherichia coli*. *J. Biol. Chem.* 281, 16879–16887.
- (37) Lee, H. I., Thrasher, K. S., Dean, D. R., Newton, W. E., and Hoffman, B. M. (1998)  $^{14}\text{N}$  electron spin-echo envelope modulation of the  $S = 3/2$  spin system of the *Azotobacter vinelandii* nitrogenase iron-molybdenum cofactor. *Biochemistry* 37, 13370–13378.
- (38) Sun, L., Groover, O. A., Canfield, J. M., and Warncke, K. (2008) Critical role of arginine 160 of the EutB protein subunit for active site structure and radical catalysis in coenzyme B<sub>12</sub>-dependent ethanolamine ammonia-lyase. *Biochemistry* 47, 5523–5535.
- (39) Benda, R., Tse Sum Bui, B., Schunemann, V., Florentin, D., Marquet, A., and Trautwein, A. X. (2002) Iron-sulfur clusters of biotin synthase in vivo: a Mössbauer study. *Biochemistry* 41, 15000–15006.
- (40) Cosper, M. M., Jameson, G. N. L., Eidsness, M. K., Huynh, B. H., and Johnson, M. K. (2002) Recombinant *Escherichia coli* biotin synthase is a  $[2\text{Fe-2S}]^{2+}$  protein in whole cells. *FEBS Lett.* 529, 332–336.
- (41) Ollagnier-de Choudens, S., Sanakis, Y., Hewiston, K. S., Roach, P., Baldwin, J. E., Munck, E., and Fontecave, M. (2000) Iron-Sulfur Center of Biotin Synthase and Lipoate Synthase. *Biochemistry* 39, 4165–4173.
- (42) Tse Sum Bui, B., Florentin, D., Marquet, A., Benda, R., and Trautwein, A. X. (1999) Mössbauer studies of *Escherichia coli* biotin synthase: evidence for reversible interconversion between  $[2\text{Fe-2S}]^{2+}$  and  $[4\text{Fe-4S}]^{2+}$  clusters. *FEBS Lett.* 459, 411–414.
- (43) Tse Sum Bui, B., Benda, R., Schunemann, V., Florentin, D., Trautwein, A. X., and Marquet, A. (2003) Fate of the  $(2\text{Fe-2S})^{2+}$  cluster of *Escherichia coli* biotin synthase during reaction: a Mössbauer characterization. *Biochemistry* 42, 8791–8798.
- (44) Gurbiel, R. J., Batie, C. J., Sivaraja, M., True, A. E., Fee, J. A., Hoffman, B. M., and Ballou, D. P. (1989) Electron-nuclear double resonance spectroscopy of  $^{15}\text{N}$ -enriched phthalate dioxygenase from *Pseudomonas cepacia* proves that two histidines are coordinated to the  $[2\text{Fe-2S}]$  Rieske-type clusters. *Biochemistry* 28, 4861–4871.
- (45) Lu, T. T., Huang, H. W., and Liaw, W. F. (2009) Anionic mixed thiolate-sulfide-bridged Roussin's red esters  $[(\text{NO})_2\text{Fe}(\mu\text{-SR})(\mu\text{-S})\text{Fe}(\text{NO})_2]^-$  (R = Et, Me, Ph): a key intermediate for transformation of dinitrosyl iron complexes (DNICs) to  $[2\text{Fe-2S}]$  clusters. *Inorg. Chem.* 48, 9027–9035.
- (46) Cicchillo, R. M., and Booker, S. J. (2005) Mechanistic investigations of lipoic acid biosynthesis in *Escherichia coli*: both sulfur atoms in lipoic acid are contributed by the same lipoyl synthase polypeptide. *J. Am. Chem. Soc.* 127, 2860–2861.
- (47) Cicchillo, R. M., Iwig, D. F., Jones, A. D., Nesbitt, N. M., Baleanu-Gogonea, C., Souder, M. G., Tu, L., and Booker, S. J. (2004) Lipoyl synthase requires two equivalents of S-adenosyl-L-methionine to synthesize one equivalent of lipoic acid. *Biochemistry* 43, 6378–6386.
- (48) Cicchillo, R. M., Lee, K. H., Baleanu-Gogonea, C., Nesbitt, N. M., Krebs, C., and Booker, S. J. (2004) *Escherichia coli* lipoyl synthase binds two distinct  $[4\text{Fe-4S}]$  clusters per polypeptide. *Biochemistry* 43, 11770–11781.
- (49) Douglas, P., Kriek, M., Bryant, P., and Roach, P. L. (2006) Lipoyl synthase inserts sulfur atoms into an octanoyl substrate in a stepwise manner. *Angew. Chem., Int. Ed.* 45, 5197–5199.
- (50) Hernandez, H. L., Pierrel, F., Elleingand, E., Garcia-Serres, R., Huynh, B. H., Johnson, M. K., Fontecave, M., and Atta, M. (2007) MiaB, a bifunctional radical-S-adenosylmethionine enzyme involved in the thiolation and methylation of tRNA, contains two essential  $[4\text{Fe-4S}]$  clusters. *Biochemistry* 46, 5140–5147.
- (51) Lee, K. H., Saleh, L., Anton, B. P., Madinger, C. L., Benner, J. S., Iwig, D. F., Roberts, R. J., Krebs, C., and Booker, S. J. (2009) Characterization of RimO, a new member of the methylthiotransferase subclass of the radical SAM superfamily. *Biochemistry* 48, 10162–10174.
- (52) DeLano, W. L. (2002) The PyMOL Molecular Graphics System.